Deep-learning based automatic segmentation of vesicles in cryo-electron tomograms

This manuscript ([permalink](#)) was automatically generated from [elatella/deep-prepyto-paper@5f5a325](#) on July 15, 2022.

Authors

- **Amin Khosrozadeh**[*]
  [XXXX-XXXX-XXXX-XXXX](#) · [ameen-khosrowzadeh](#)
  Institute of Anatomy, University of Bern, Bern, Switzerland; Graduate School for Cellular and Biomedical Sciences, University of Bern · Funded by Grant XXXXXXXX

- **Raphaela Seeger**[*]
  [XXXX-XXXX-XXXX-XXXX](#) · [elatella](#)
  Institute of Anatomy, University of Bern, Bern, Switzerland; Graduate School for Cellular and Biomedical Sciences, University of Bern

- **Julika Radecke**
  [0000-0002-5815-5537](#) · [julikaradecke](#)
  Institute of Anatomy, University of Bern, Bern, Switzerland; Department of Neuroscience, Faculty of Health and Medical Science , 2200 Copenhagen N, University of Copenhagen, Copenhagen, Denmark; Diamond Light Source Ltd, Didcot, Oxfordshire, United Kingdom

- **Guillaume Witz**
  [0000-0003-1562-4265](#) · [guiwitz](#)
  Science IT Service, University of Bern, Bern, Switzerland; Microscopy Imaging Center, University of Bern, Bern, Switzerland

- **Jakob B. Sørensen**
  [0000-0001-5465-3769](#) · [JBSorensen](#)
  Department of Neuroscience, University of Copenhagen, Blegdamsvej 3B, 2200 Copenhagen N, Denmark · Funded by Novo Nordisk Fonden, NNF17OC0028516.; Carlsbergfondet, CF17-0875; Independent Research Fond Denmark, 8020-00228A; Lundbeckfonden, R277-2018-802

- **Benoît Zuber**[✉]
  [0000-0001-7725-5579](#) · [aseedb](#)
  Institute of Anatomy, University of Bern, Bern, Switzerland · Funded by Swiss National Science Foundation, 179520; ERA-NET NEURON, NEURON-119

✉ Address correspondence to benoit.zuber@ana.unibe.ch.

* These authors contributed equally.

Abstract

Cryo-electron Tomography (Cryo-ET) has the potential to reveal cell structure down to atomic resolution. Nevertheless, cellular cryo-ET data is often highly complex and visualization, as well as quantification, of subcellular structures require image segmentation. Due to a relatively high level of noise and to anisotropic resolution in cryo-ET data, automatic segmentation based on classical computer vision approaches usually does not perform satisfyingly. For this reason, cryo-ET researchers have mostly performed manual segmentation.

Communication between neurons rely on neurotransmitter-filled synaptic vesicle (SV) exocytosis. Recruitment of SVs to the plasma membrane is an important means of regulating exocytosis and is influenced by interactions between SVs. Cryo-ET study of the spatial organization of SVs and of their interconnections allows a better understanding of the mechanisms of exocytosis regulation. To obtain a faithful representation of SV connectivity state, an absolutely vital prerequisite is an extremely accurate SV segmentation. Hundreds to thousands of SVs are present in a typical synapse, and their manual segmentation is a burden. Typically accurately segmenting all SVs in one synapse takes between 3 to 8 days. This segmentation process has been widely recognized as a bottleneck by the community.

Several attempts to automate vesicle segmentation by classical computer vision or machine learning algorithms have not yielded very robust results. We addressed this problem by designing a workflow consisting of a U-Net convolutional network followed by post-processing steps. This combination yields highly accurate results. Furthermore, we provide an interactive tool for accurately segmenting spherical vesicles in a fraction of the time required by available manual segmentation methods. This tool can be used to segment vesicles that were missed by the fully automatic procedure or to quickly segment a handful of vesicles, while bypassing the fully automatic procedure. Our pipeline can in principle be used to segment any spherical vesicle in any cell type as well as extracellular vesicles.

Introduction

The fine architecture of cells can be investigated by cryo-electron tomography (cryo-ET) [1]. Cellular structures are preserved down to the atomic scale through vitrification and observation of the samples in a fully hydrated state. When a macromolecule is present in a sufficient number of copies in the cells imaged by cryo-ET, it is possible to obtain its atomic structure in situ using subtomogram averaging [2,3]. Cellular cryo-ET datasets are usually extremely complex, making them difficult to analyze. This is aggravated by the sensitivity of biological samples to electron radiation, which limits the signal-to-noise ratio in cryo-ET datasets [4]. Tomographic reconstructions are generated from a series of images of the sample acquired at different viewing angles. The geometry of the samples prevents acquisition at certain angles, resulting in anisotropic spatial coverage. The resolution in the directions close to the axis of the electron beam incident on the untilted sample is strongly reduced. This effect, commonly referred to as the missing-wedge artifact, further complicates data analysis. In particular, organelles fully bounded by a membrane appear to have holes at their top and bottom (relative to the electron beam axis) [4].

The synapse is the functional cellular contact at which information is transmitted from a neuron to another. The former neuron is called presynaptic and the latter is postsynaptic. In most cases, the signal is transmitted by the release of neurotransmitters into the intercellular space. Neurotransmitters are stored in SVs and are released following the fusion of a vesicle with the presynaptic plasma membrane. A synapse contains hundreds of SVs and their mobility and recruitability for neurotransmitter release depends on inter-vesicle interactions through so-called connector structures [5]. The characterization of these interactions can be performed automatically

with the pyto software, which implements a hierarchical connectivity approach to detect and annotate connectors [6]. For accurate connector segmentation, an exceptionally precise segmentation of SVs is prerequisite. To date, this SV segmentation has been achieved manually, but given the massive number of SVs per dataset, it is an extremely time-consuming process. Typically, one person spends 3 to 8 working days to segment a single dataset. Attempts to perform this task automatically based on classical computer vision algorithms have not yielded sufficiently accurate performance [7]. To alleviate this situation, we considered applying deep learning methods.

Convolutional neural networks (CNN) have been successfully employed to segment cryo-ET data [8]. Although entirely satisfying for visualization purposes, this approach has not met the requirements of pyto. A recent publication described accurate SV segmentation of transmission electron microscopy images using CNN, but it is limited to 2-dimensional images of resin-embedded synapses [9]. For our use-case, a common issue is that the input data consists of 2-dimensional images. In the first study, cryo-ET data are decomposed in individual 2-dimensional slices, which are handed as seperate input to the CNN. The independent output prediction images are re-assembled in a 3-dimensional stack.[8] As discussed above, membranes oriented approximately parallel to the plane of the 2-dimensional tomographic images are not resolved. In the absence of contextual knowledge of the other 2-dimensional images, the CNN fails to segment these regions of the vesicles. Hence, spherical vesicles appear open, whereas we expect closed spherical objects. To overcome this limitation, we used a U-Net CNN that takes 3-dimensional images as input. U-Net architecture has been introduced in 2015 by Ronenberger et al. [10]. It consists of a contracting path, typical of CNN, and a symmetric expanding path. At each expansion step, the correspondingly cropped feature map of the contracting path is concatenated. The contracting path captures context, while the expanding path coupled with concatenation enables precise localization. The U-Net architecture was developed to achieve a fast and accurate segmentation of biomedical two-dimensional images, with the requirement of only a small fraction of training data in comparison to previous CNNs. *might be redundant* Arranging the sequence of convolution layers in the contraction path along with skip connection and concatenating into the expansion path bring significant privilege for medical and semantic segmentation. Concurrent with the appearance of 3D convolutional neural networks (CNN) three-dimensional form of U-Net was also developed for volumetric image analysis.

It was then extended to segment 3-dimensional biomedical images (3D U-Net) [11]. Weigert et al. [12] implemented a U-Net for content-aware restoration (CARE) of 3-dimensional fluorescence microscopy datasets. They showed that it can restore information from anisotropic and very noisy datasets.

We implemented a 3D U-Net based on CARE building blocks and trained it with manually segmented datasets. This method provided good accuracy and was only slightly affected by the missing wedge artifact. Nevertheless, it was not quite sufficient for our downstream pyto analysis. Hence, we developed a post-processing method, which transforms the segmented objects into spheres and refines their radius and center location. This leads to a substantial accuracy improvement, which are reflected in better pyto performance. Additionally, we designed a multivariate ranking procedure, highlighting possibly wrongly segmented SVs. We also introduce a semi-automatic method to very quickly fix wrongly segmented and missed SVs.
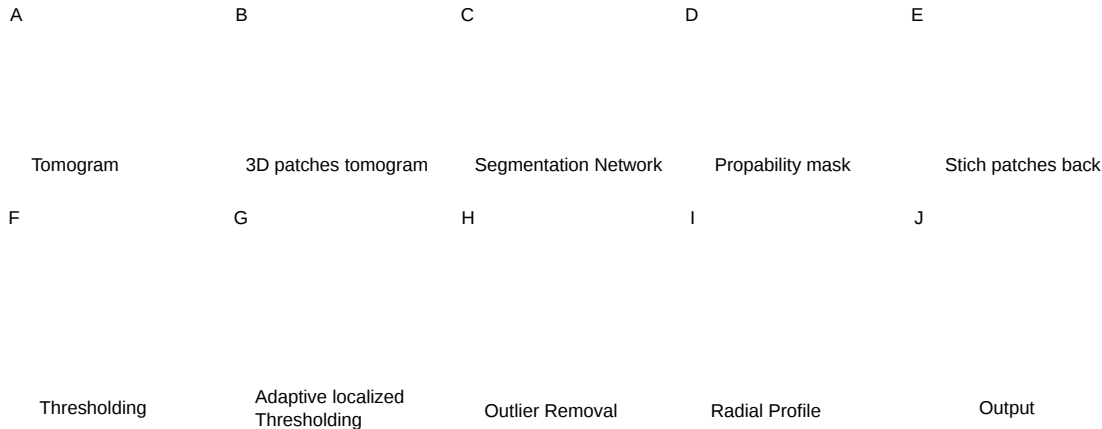
Although our set of procedures was developed with the use case of SV segmentation in mind, it can be used to segment any other types of biological spherical vesicles, such as transport vesicles, secretory vesicles, endocytic vesicles, and extracellular vesicles.

Results

To automize the tracing of cellular features in tomograms, also called segmentation, we developed a deep-learning pipeline, which segments 3D objects. -> similar approaches in 2D The manual

segmentation of synaptic vesicles is one of the most time-intensive steps, when segmenting tomograms of presynaptic terminals. Synaptic vesicles also constitute a large, homogeneous group, which would create a large training set for deep learning applications. Therefore, we decided to develop the automatic segmentation for synaptic vesicles in an initial step. The used tomograms were previously manually segmented with IMOD [13]. In a next step, filaments connecting the synaptic vesicles with each other (connectors) and to the active zone (AZ) were automatically segmented with the algorithm application Pyto [6].

A	B	C	D	E
Tomogram	3D patches tomogram	Segmentation Network	Propability mask	Stich patches back

| F	G	H	I	J
Thresholding	Adaptive localized Thresholding	Outlier Removal	Radial Profile	Output

Figure 1: Pipeline of automatic segmentation. a) tomograms b) patchify the tomograms into 3D patches c) Segmentation Network d) probability masks e) stitching patches back f) thresholding g) adaptive localized thresholding h) outlier removal i) radial profile
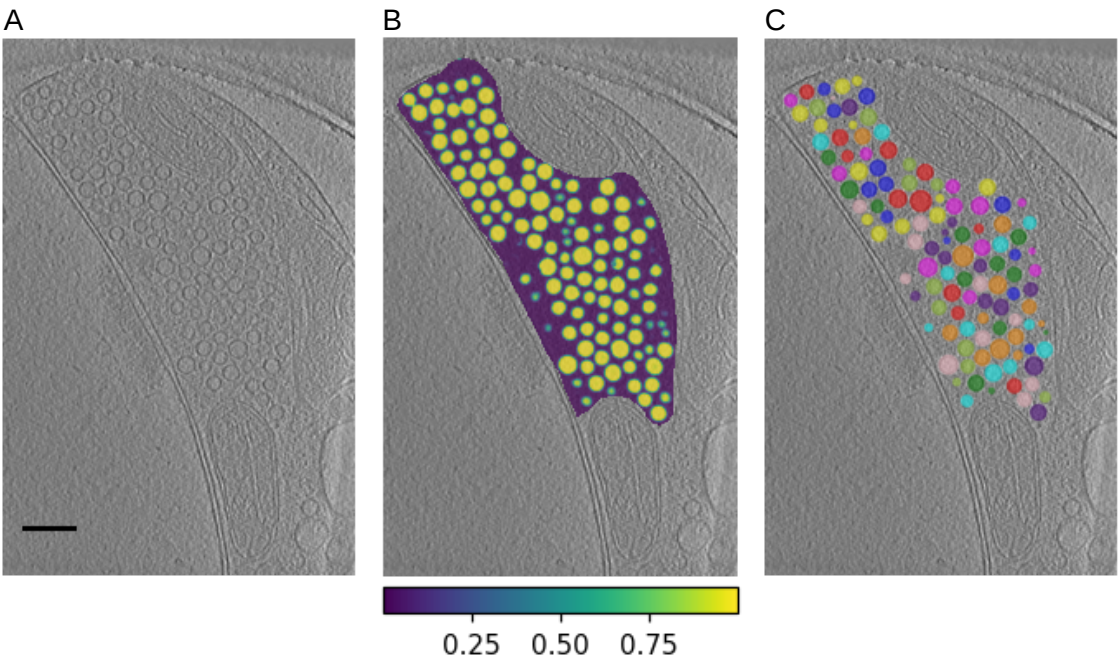
Figure 2: 2D Slices A) a section from z axis of a tomogram's presynaptic terminal of a neuron B) instance mask of the vesicles after post processing C) predicted probability mask by the segmentation network

![**Dice Imporvment** Dice improvements after post processing of initial predicted mask (different colors correspond to different tomograms): a) training datasets b) synaptosome test datasets c) Neuron test datasets(images/improvment-neurons.png){#fig:tom width="15cm"}
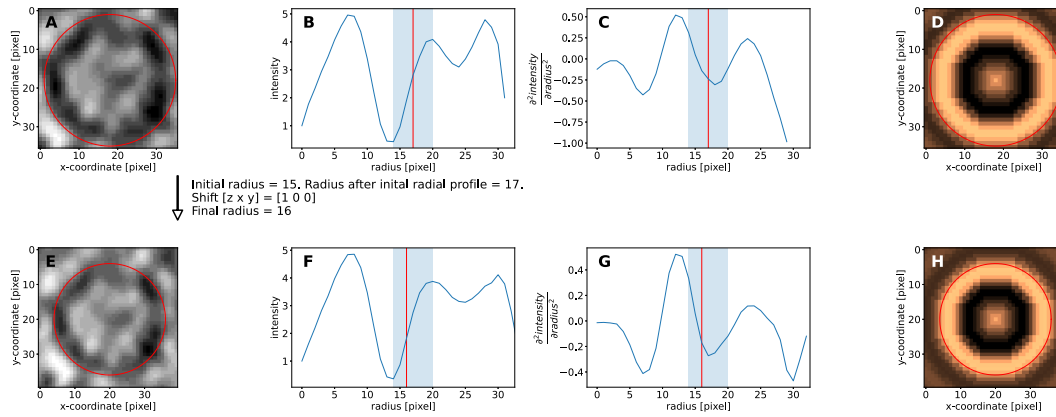
Figure 3: Vesicle radius and position through radial profile and cross-correlation Radial Profile Refinement A) couple of vesicles are not centered B) Radial Profile. Blue range is from membrane center to outer white halo center, this is the search range for the optimal radius. (smoothed by gaussian filtering) C) second derivative of radial profile E, F, H, G) Same as above columns after refinement

Fig 6- Splitting adjacent vesicles. A) Examples of tomogram, no labels; B) raw label with connected vesicle-labels; C) modified label with seperated vesicles —> for software: IMOD

Comparison of manual segmentation with automatic deep-learning based segmentation
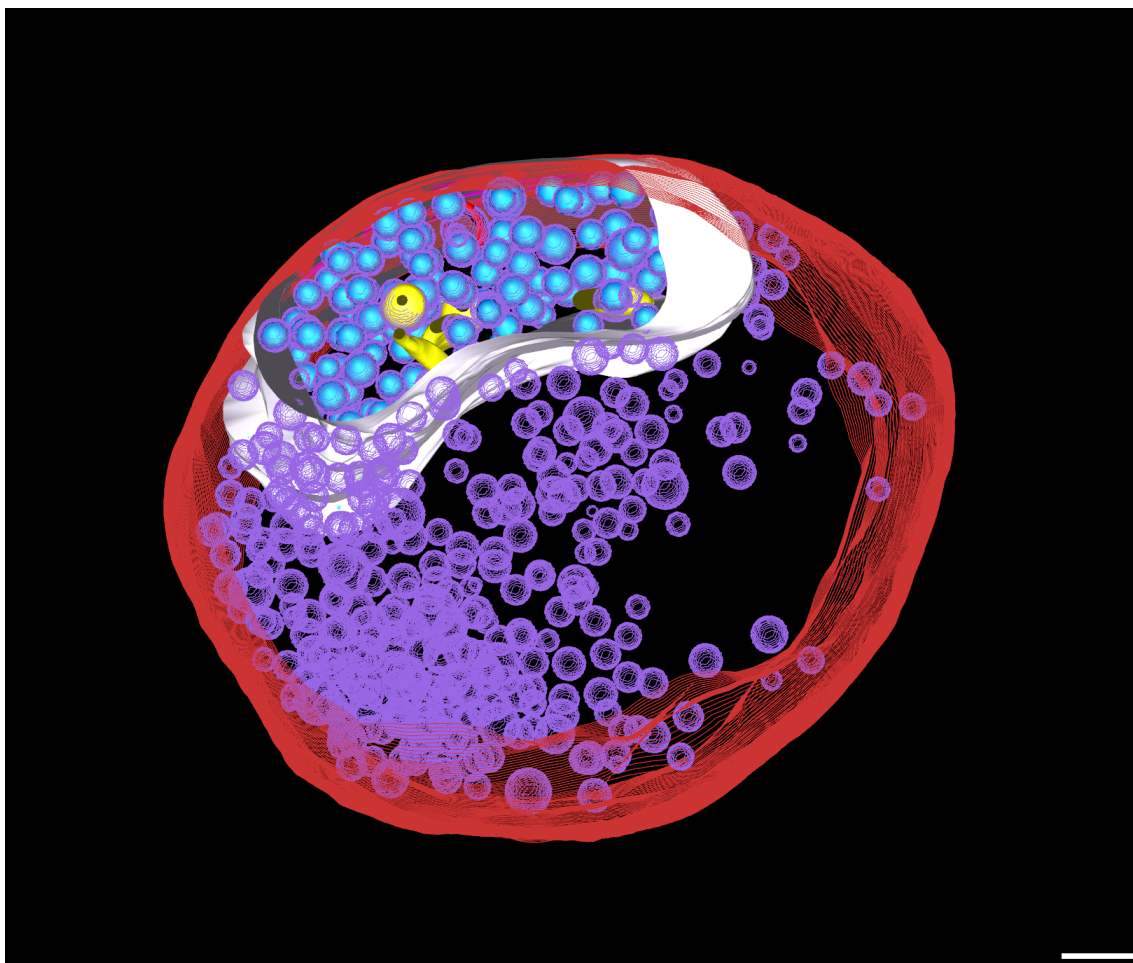
Figure 4: 3D model of manual segmented and automatically segmented synaptosome.

Evaluation metric DICE for pixel/pixel analysis

Table 1- Evaluation of the segmentation- MDICE: Mask Dice coefficient for the predicted mask PDICE: Dice coefficient after post-processing SIGMA-d: diameter error on correctly detected vesicle, DELTA-c: average error center (nm) #Vesicles: number of expected vesicles TP: True Positive FN: False Negative FP: False Positive

Final Eval Tables

Train Dataset

Dataset	Mask DICE	Final Label DICE	δ d	Δ c (nm)	# of Vesicles	TP	FN	FP
Synaptosome C1	0.44	0.73	0.07	2.55±1.56	223	198	26	49
Synaptosome C2	0.8	0.9	0.05	2.12±1.06	105	103	2	1
Synaptosome C3	0.67	0.9	0.05	1.86±1.24	128	127	1	6
Synaptosome C4	0.62	0.89	0.03	1.78±0.92	144	141	3	4
Synaptosome C5	0.58	0.87	0.04	1.86±1.00	214	209	5	13
Synaptosome C6	0.56	0.84	0.04	1.92±1.05	104	102	2	16
Synaptosome C7	0.78	0.88	0.06	1.86±0.90	184	184	0	16
Synaptosome C8	0.75	0.9	0.05	1.70±0.93	132	126	6	1
Synaptosome C9	0.59	0.87	0.05	1.87±0.91	135	132	3	14
Average	**0.64±0.11**	**0.86±0.05**	**0.05**	**1.95±1.08**	**152.22**	**97.00%**	**3.00%**	**7.30%**

Test Dataset (Same preparation and microscope with training set)

Dataset	Mask DICE	Final Label DICE	δ d	Δ c (nm)	# of Vesicles	TP	FN	FP
Synaptosome C10	0.75	0.88	0.07	1.86±1.18	129	123	6	5
Synaptosome T1	0.75	0.83	0.11	2.66±1.52	699	687	12	33
Synaptosome T2	0.74	0.77	0.11	2.27±1.84	122	117	5	2
Synaptosome T3	0.72	0.74	0.11	3.64±2.22	434	397	37	57
Synaptosome T5	0.77	0.85	0.08	2.20±1.26	535	526	9	25
Synaptosome T6	0.6	0.83	0.07	2.02±1.12	373	353	20	42
Synaptosome T7	0.8	0.83	0.06	2.22±1.14	110	107	3	9
Synaptosome T8	0.83	0.91	0.04	2.09±1.04	100	99	1	2
Synaptosome T10	0.77	0.86	0.05	1.96±1.04	77	74	3	6
Average	**0.75±0.06**	**0.83±0.05**	**0.08**	**2.32±1.43**	**286.56**	**96.30%**	**3.70%**	**6.10%**

Test Dataset 3 (Neuron Dataset)

Dataset	Mask DICE	Final Label DICE	δ d	Δ c (nm)	# of Vesicles	TP	FN	FP

Dataset	Mask DICE	Final Label DICE	δ d	Δ c (nm)	# of Vesicles	TP	FN	FP
Neuron 133	0.76	0.86	0.05	2.16±1.32	523	467	56	8
Neuron 123	0.64	0.71	0.05	2.05±1.18	66	58	8	2
Neuron 84	0.86	0.89	0.06	1.44±0.75	498	484	14	1
Neuron 134	0.56	0.67	0.09	2.87±2.50	638	384	254	63
Neuron 115	0.57	0.63	0.08	3.56±3.23	170	123	47	32
Neuron 102	0.73	0.86	0.05	1.47±0.79	103	86	17	1
Neuron 80	0.7	0.81	0.07	2.67±2.00	111	102	9	3
Neuron 114	0.65	0.73	0.07	2.68±1.79	131	93	38	9
Neuron 132	0.69	0.87	0.03	1.65±1.26	135	129	6	32
Neuron 73	0.78	0.83	0.06	2.93±2.00	526	483	43	2
Neuron 128	0.67	0.85	0.04	2.33±1.70	252	232	20	19
Neuron 116	0.62	0.73	0.07	2.38±1.82	296	207	89	35
Average	**0.69±0.09**	**0.79±0.09**	**0.06**	**2.35±1.83**	**287.42**	**83.60%**	**16.40%**	**7.90%**

Global analysis
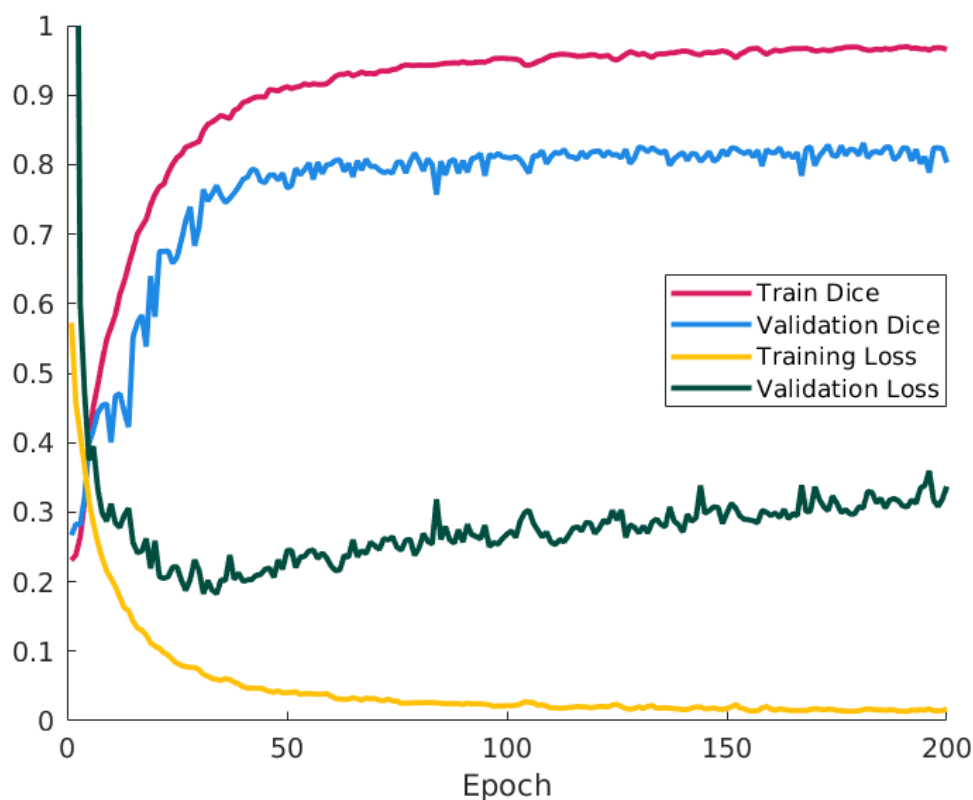
Figure 5: Dice coefficient and loss value for training and validation set.

3d unet good for 3D processing recent Nature methods paper by Ben Engel, DeepFinder -> Relion for STA creates mask to find more using dl -what are they doing, maybe compare that in the text, different aims; we might compare results we achieve (keep as bonus, revision)

3 different types of dl: classification, localization and segmentation We specialize in accurately segmenting 3D svs -> results through the network, output is a mask, smooth DICE/ binary DICE =

which one for our mask? one function for both? -> Amin will check when we encounter error until now we remove sv(?), bug inside function -> fix bug for better performance, how many fail and why? evaluation: objectwise evaluation for I/O, radius, center (according to nature paper) -> compare with manual seg other common evaluation tool other than DICE (Amin wants to check)

Discussion

DICE

Outlook

implement automatic cell-outline and active zone segmentation as deep learning workflow using UNet implement automatic connector and tether segmentation as a deep leaning workflow using UNet

Materials and methods

Cryo-electron Tomography Datasets

Two datasets of different origin were used as input and test subjects for the automatic segmentation pipeline, rat synaptosomes as well as astrocytic and neural cell cultures derived from mice. Both datasets have been previously analyzed [14].

Rat synaptosomes

The preparation of the rat synaptosomes were previously described [15]. After the purification, the synaptosomes were incubated for 30min at room temperature. 1.3mM CaCl2 and 10 nm gold fiducials were added (gold fiducials, #s10110/8. AURION Immuno Gold Reagents & Accessories. Wageningen, The Neatherlands). The synaptosome solution was applied to a 200-mesh lacey finder carbon film grid (#AGS166-H2. Agar Scientific. Elektron Technology UK Ltd. Stansted, UK). Manual blotting was used to remove exess liquid with the aid of a filter paper. Thereafter the grid was immediately plunge frozen in liquid ethane using a homebuilt plunge freezer controlled with a LabView script (National Onstruments Corporation. Mopac Expwy Austin, TX, USA). The grids coated with rat synaptosomes were mounted in a cryo-holder (Gatan, Pleasonton, CA, USA) and transferred to a Tecnai F20 (FEI, Eindhoven, The Netherlands) which was set to low dose conditions, operated at 200 kV, and equipped with a field emission gun. Images were recorded with a 2k x 2k CCD camera (Gatan) mounted after a GIF Tridiem post-column filter (Gatan) operated in zero-loss mode. The sample was kept at about -180°C. Tilt series were acquired using SerialEM [16] for automated acquisition recorded typically from -50° to 50° with a 2° angular increment and an unbinned pixel size of 0.75 or 1.2 nm. Due to sample thickness (400-700 nm), tomograms were usually not recorded with higher tilt angles. Defocus was set between -8 to -12 μm and the total electron dose used was about 80-100 e$^-$/Å^2. Some tomograms were acquired at a Titan Krios equipped with a K2 direct electron detector (Gatan) without energy filter. The K2 camera was operated in superresolution counting mode and between 8-40 frames per tilt angle were taken. Tilt series were acquired using the Latitude software (Gatan) for automated acquisition recorded typically from -60° to 60° with a 2° angular increment and an unbinned pixel size of 0.6 nm. Defocus was set between -8 to -12 μm and the total electron dose used was about 80-100 e$^-$/Å^2. Prior to image processing the frames at each tilt angle, frames were aligned and averaged in 2dx MC_Automator [17] with motioncor [18]. 3D reconstruction was done in IMOD [13]. The alignments were done using the automated fiducial tracking function and the 3D reconstructions were done using the weighted back projection followed by a nonlinear anisotropic diffusion (NAD) filtering.

Astrocytic and neuronal mouse culture

The preparation of astrocytic and neuronal culture has been published before [19]. After 12 to 14 days of incubation grids with mouse neurons were plunge frozen with a Vitrobot (Thermofisher Scientific, Mark IV) with a blot time of 3 s and a blot force of -10. Wait time and drain time were not used. Humidity was set to 100% at 4°C. 4 µl undiluteted 10 nm BSA gold tracer (Aurion) was added directly onto the grid prior to plunge freezing. Cultured mouse neurons tilt series were acquired at a Titan Krios, equipped with a Falcon 3 direct electron detector (Thermofisher Scientific) without energy filter. The Falcon camera was operated in linear mode. Tilt series were acquired using the TEM Tomography software (TFS) for automated acquisition recorded typically from -60° to 60° with a 2° angular increment and an unbinned pixel size of 0.37 nm. Defocus was set between -6 to -10 µm and the total electron dose used was about 80-100 e⁻/Å². Tomogram reconstruction was done in the same way as for the synaptosome datasets.

Manual segmentation procedures

Manual segmentation of SVs, mitochondria, and the active zone PM was done in IMOD (Figure S4A&B). The boundary marked the region to be analyzed by Pyto [6]. The analysis by Pyto was essentially the same as described previously [5,6].

In short, the segmented area is divided in 1 voxel thick layers parallel to the active zone for distance calculations. A hierarchical connectivity segmentation detects densities interconnecting vesicles (so called connectors) and densities connecting vesicles to the active zone PM (so called tethers) (Figure `\_add figure number*`). Distance calculations are done with the center of the vesicle. Mainly default settings were used. The segmentation procedure is conservative and tends to miss some tethers and connectors because of noise. Consequently, the numbers of tethers and connectors should not be considered as absolute values but rather to compare experimental groups. As it was done before, an upper limit was set between 2100 and 3200 nm³ on segment volume. The tomograms that were used for this analysis were binned by a factor of 2 to 3, resulting in voxel sizes between 2.1 and 2.4 nm.

Pre-processing of manual segmentation outputs from IMOD for further use (jupyter notebook pre-pyto)

Description of Machine Learning

This experiment was conducted on a workstation with an AMD Ryzen Threadripper 3970X CPU with a NVIDIA GeForce RTX 2080 Ti GPU. All the framework has been implemented in Python using the Keras library (2.4.3) and Tensorflow (2.4.1). The workflow includes a GUI based on a multi-dimensional image viewer, Napari (0.4.15), enabling the user to add and remove vesicles. `\_any other packages required?*`

The used datasets included a total of 30 tomograms with heterogeneous pixel sizes, defocus and resolution.

Deep Model Training with a 3D U-Net

Create an Input Voxel Patch

The training set was prepared by splitting the 3D tomographic volume into 32x32x32 `\_voxels??*` sub volumes and keeping only volumes occupied by a sufficient amount (> 1000 voxels) of binarized

vesicle labels. The obtained sub volumes were randomly divided into ten subsets of the training set, this method is termed k-fold cross-validation in the field of machine learning. All of these subsets or "folds" were used as training sets, as an entirely seperate set of tomographic subvolumes was used for validation, to avoid overfitting.

`\_are the folds overlapping? are the tomograms normalized any further than the NAD from previous segementation before feeding it to the deeplearning model? add image from odt??, the 2D slices of the subset are supposed to be 32x32x32, but seem to have a different size... padding?? ---> results*`

3D U-Net architecture

The previously prepared subsets are fed into the 3D U-Net in batches of 50. `\_cite Ronneberger, what was changed compared to the original U-Net, is there a better publication to cite?*` These were passed throught the U-Net in a total of 200 epochs. Batch normalization was applied before Rectified Lienear Unit (ReLU) activation `\_was it? cite Ioffe & Szegedy, maybe? [@doi:10.48550/arXiv.1502.03167]*`.

The 3D U-Net architecture is composed of a contracting or analysis path (convolutional layers), and expanding or synthesis path (deconvolutional layers) (Figure 6). `\_did we wrote our own U-Net or do we need to quote someones github for the original framework*`
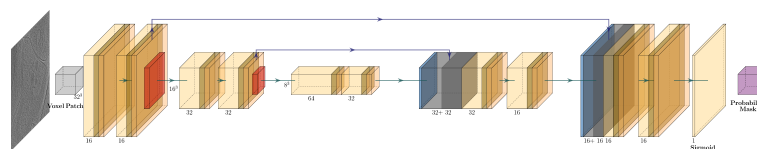
Figure 6: Segmentation Network: U-Net. Input Size is 32^3 `\_voxels??*`, in each resolution we have two convolution layer followed by batch normalization layer and rectified Linear Units (ReLU) activation function. Intermediate sizes are written on top of arrows, number of convolution filters is written bottom of boxes. Skip connections shows concatenation of the features from contracting path (left side of the network) and expansive path (right side of the network). `\_explain different colors, do they correspond with the different steps? for example: red- max pooling 2x2x2? add figure legend?*`

`\_what do we use as initial encoder weights and backbone*` During each layer of the analysis path, the convolution filter consiting of a 3x3x3 kernel, with randomly initialized weights, was moved over all the voxels in each subset twice, each time taking their dot product. This kernel extracts and enhances the features in different parts of the image. This is followed by a ReLU function, which can be described as

$$f(x) = max(0, x)$$

which will output the positive input directly, while setting negative input to 0.

Between each layer, the voxels were condensed, or downsampled, via a max-pooling step of 2x2x2, in which the maximum value of the 2x2x2 voxel cube is put forth. With every layer of the U-Net, the input size thereby halfs, while the number of channels doubles.

While the analysis path focusses on the identification of what to segement, the synthesis part focusses on their localization. The synthesis path of the U-Net uses the same basic architecture as the analysis path, with a slight variation of using up convolution operation and implementing skip connections, where feature maps of the analysis part are concatunated to the output of the transposed convolutions of the same level.

The sigmoid activation function is the last block of the U-Net (Figure 6), it triggers the loss function, which As the segementation of vesicles can be considered a binary classification task, binary cross-entropy was implemented as a loss function.

$$Loss = -\frac{1}{outputsize} \sum_{i=1}^{outputsize} y_i * log\hat{y}_i + (1 - y_1) * log(1 - \hat{y}_1)$$

with the *output size* being the nuber of scalar values in the model output, $\hat{y}\_1\_$ being the *i*-th scalar value in the model output and $y\_i\_$ being the corresponding target value. `\_publication to cite? *`

The binary cross-entropy lossfunction converts the output from the decoder path into a mask, where each voxel is assigned as either vesicle or not-vesicle.

training: weights -> Adam optimizer for the training of the network [20].

"The back-propagation is done to update the weights and reduce the loss function with the help of an optimizer - the most common optimizer algorithm is gradient descent. Multiple epochs are run until the loss converges to the global minima."

Come after the convolutional layers to achieve a 3D probability mask a Softmax layer applies to bring channel size to one.

Mask prediction

We split large tomograms into 32x32x32 patches with step size of 24 (stride) and then stitch together the predictions to get the final probability mask.

Transfer Learning

Postprocessing

Estimating Global Threshold

In order to binarize the obtained probability mask, we search through some thresholds (from 0.8 to 1.0) and select the one that minimizes something. `\_add image from odt??*`

Adaptive Localized Threshold

although the global threshold reveals almost all desired synaptic vesicles due to variation in the intensity of vesicles surrounding some binarized labels that are far away from the spherical shape of vesicles. First, by looking at the extent value(Ratio of pixels in the region to pixels in the total bounding box. Computed as area / (rows * cols)) and the size of each particle's binary label we can capture those vesicles that are get connected and those vesicles that captured partially. Then by searching more into the probability mask, we try to expand the partially detected vesicles and separate those close connected vesicles by searching between the initial threshold and one to find a better finner threshold that can separate these vesicles.

Radial Profile

Outlier Removal

We define feature space on predicted vesicles' label containing thickness, membrane density, and estimated radius of a vesicle. (Benoit: after radial profile, we can add the definition of thinness and membrane as well) While we face different metrics for detecting outliers we apply Mahalanobis Distance MD on this multivariate space MD to calculate L2 norm distance on normalized variable using the covariance matrix of observation. Afterward, we calculate the p-value of MD and bring this evaluation setup in iterative form while giving the second chance to detect outlier vesicles while recalculating radial profile in a specific margin range (0-10) and removing them if they could not pass a margin on the p-value.

Radius Estimation (Cross Correlation through Radial Profile)

Analysis of Results

We design the evaluation framework to show robust capabilities of the proposed toolbox on synaptic vesicles segmentation which not only to be content with quantitative evaluation on the neural network performance but rather assay the segmentation of vesicles in practice and using the output of the segmentation with another pre-developed toolbox for segmenting tethers and connectors in presynaptic.

1. Dataset: All tomograms that we partially segmented and used for training (Synaptosome)
2. A single tomogram with the exactly same setup and sample preparation like the train dataset
3. Dataset: 8 Synaptosome tomogram with ground truth (with an exceeding treatment on the samples)
4. Dataset: 12 Neuron fully segmented tomograms with completely different sample preparation and microscope setup

DICE

The quantification of the performance of the model while training is calculated with the general form of dice coefficient for the probabilistic maps and after stitching the probabilistic mask of patches back together and building the tomogram probabilistic map we have another calculation on the whole tomogram for evaluating the similarity of the predicted probability mask with ground truth. The binarization from the same formulation converges to this interpretation that we measure the overlap between two samples.

$$1 - \frac{2 \sum_{pixels} y_{true} y_{pred}}{\sum_{pixels} y_{true}^2 + \sum_{pixels} y_{pred}^2}$$

`\_shouln't it be voxels instead of pixels??*`

We monitored all the stages of post-processing on the eventual label file with DICE to see the effect of each post-processing step and we report the final label's DICE.

However dice coefficient is a good global measure to assess our prediction in comparison to ground truth but it is far away from how individually vesicles are segmented. For example, a single generated vesicle label containing several close connected vesicles would not be practical for further analysis for the researcher although it could have almost the same dice value. What is important for actual usage of the software would be the number and percentage of true-detected vesicles, false-positive and false-negative rates. We can also calculate the error of the estimated diameter and center. We define a vesicle as a true-detected vesicle if the predicted center is in the hand-segmented vesicle and the other way around the center of prediction is in the predicted vesicle. This means the volume of intersection of the estimated vesicle with the distance of d to a ground truth vesicle with radius R is:

$$V = \frac{1}{12}\pi(4R + d)(2R - d)$$

Diameter Error

The relevant characterization of each vesicle would diameter of vesicles which also we used to remove outliers as well (radius of vesicles in that case). The error of diameter estimation of true-detected vesicle is defined as 1 minus the proportion of diameters

$$\delta d = 1 - \frac{min(dSi, dGTi)}{max(dSi, dGTi)} \tag{1}$$

where dGTi diameter of each true manual segmented vesicle, and dSi is the diameter of its estimation.

Center error

The center error is a euclidean distance of ground truth and corresponding true predicted vesicles. Besides this calculation, if we measure each axis error it will reveal that human bias in segmentation is more affected on the Z-axis. [we didn't show it in number but its checked the hypothesis]

References

1. **Towards Visual Proteomics at High Resolution**
   Felix JB Bäuerlein, Wolfgang Baumeister
   Journal of Molecular Biology (2021-10) https://doi.org/gn9t3v
   DOI: 10.1016/j.jmb.2021.167187 · PMID: 34384780

2. **Exploring high-resolution cryo-ET and subtomogram averaging capabilities of contemporary DEDs**
   Martin Obr, Wim JH Hagen, Robert A Dick, Lingbo Yu, Abhay Kotecha, Florian KM Schur
   Molecular Biology (2022-01-10) https://doi.org/gn92pd
   DOI: 10.1101/2022.01.10.475481

3. **High-resolution in situ structure determination by cryo-electron tomography and subtomogram averaging using emClarity**
   Tao Ni, Thomas Frosio, Luiza Mendonça, Yuewen Sheng, Daniel Clare, Benjamin A Himes, Peijun Zhang
   Nature Protocols (2022-02) https://doi.org/gn92pc
   DOI: 10.1038/s41596-021-00648-5 · PMID: 35022621 · PMCID: PMC9251519

4. **STRUCTURAL STUDIES BY ELECTRON TOMOGRAPHY: From Cells to Molecules**
   Vladan Lučić, Friedrich Förster, Wolfgang Baumeister
   Annual Review of Biochemistry (2005-06-01) https://doi.org/cfd27f
   DOI: 10.1146/annurev.biochem.73.011303.074112 · PMID: 15952904

5. **Quantitative analysis of the native presynaptic cytomatrix by cryoelectron tomography**
   Rubén Fernández-Busnadiego, Benoît Zuber, Ulrike Elisabeth Maurer, Marek Cyrklaff, Wolfgang Baumeister, Vladan Lučić
   Journal of Cell Biology (2010-01-11) https://doi.org/b9c26b
   DOI: 10.1083/jcb.200908082 · PMID: 20065095 · PMCID: PMC2812849

6. **Hierarchical detection and analysis of macromolecular complexes in cryo-electron tomograms using Pyto software**
   Vladan Lučić, Rubén Fernández-Busnadiego, Ulrike Laugks, Wolfgang Baumeister
   Journal of Structural Biology (2016-12) https://doi.org/f9d5t2
   DOI: 10.1016/j.jsb.2016.10.004 · PMID: 27742578

7. **Robust membrane detection based on tensor voting for electron tomography**
   Antonio Martinez-Sanchez, Inmaculada Garcia, Shoh Asano, Vladan Lucic, Jose-Jesus Fernandez
   Journal of Structural Biology (2014-04) https://doi.org/f5zkj8
   DOI: 10.1016/j.jsb.2014.02.015 · PMID: 24625523

8. **Convolutional neural networks for automated annotation of cellular cryo-electron tomograms**
   Muyuan Chen, Wei Dai, Stella Y Sun, Darius Jonasch, Cynthia Y He, Michael F Schmid, Wah Chiu, Steven J Ludtke
   Nature Methods (2017-10) https://doi.org/gkpj62
   DOI: 10.1038/nmeth.4405 · PMID: 28846087 · PMCID: PMC5623144

9. **Automated Detection and Localization of Synaptic Vesicles in Electron Microscopy Images**
   Barbara Imbrosci, Dietmar Schmitz, Marta Orlando
   eneuro (2022-01) https://doi.org/gn9n8k
   DOI: 10.1523/eneuro.0400-20.2021 · PMID: 34983830 · PMCID: PMC8805189

10. **U-Net: Convolutional Networks for Biomedical Image Segmentation**
Olaf Ronneberger, Philipp Fischer, Thomas Brox
arXiv (2015-05-19) https://arxiv.org/abs/1505.04597

11. **3D U-Net: Learning Dense Volumetric Segmentation from Sparse Annotation**
Özgün Çiçek, Ahmed Abdulkadir, Soeren S Lienkamp, Thomas Brox, Olaf Ronneberger
arXiv (2016-06-22) https://arxiv.org/abs/1606.06650

12. **Content-aware image restoration: pushing the limits of fluorescence microscopy**
Martin Weigert, Uwe Schmidt, Tobias Boothe, Andreas Müller, Alexandr Dibrov, Akanksha Jain, Benjamin Wilhelm, Deborah Schmidt, Coleman Broaddus, Siân Culley, … Eugene W Myers
Nature Methods (2018-12) https://doi.org/gfkkfd
DOI: 10.1038/s41592-018-0216-7 · PMID: 30478326

13. **Computer Visualization of Three-Dimensional Image Data Using IMOD**
James R Kremer, David N Mastronarde, JRichard McIntosh
Journal of Structural Biology (1996-01) https://doi.org/d9nfzw
DOI: 10.1006/jsbi.1996.0013 · PMID: 8742726

14. **Morphofunctional changes at the active zone during synaptic vesicle exocytosis**
Julika Radecke, Raphaela Seeger, Anna Kádková, Ulrike Laugks, Amin Khosrozadeh, Kenneth N Goldie, Vladan Lučić, Jakob B Sørensen, Benoît Zuber
Neuroscience (2022-03-07) https://doi.org/gpm26v
DOI: 10.1101/2022.03.07.483217

15. **A rapid Percoll gradient procedure for preparation of synaptosomes**
Peter R Dunkley, Paula E Jarvie, Phillip J Robinson
Nature Protocols (2008-11) https://doi.org/b7zwh8
DOI: 10.1038/nprot.2008.171 · PMID: 18927557

16. **Automated electron microscope tomography using robust prediction of specimen movements**
David N Mastronarde
Journal of Structural Biology (2005-10) https://doi.org/ff7gzx
DOI: 10.1016/j.jsb.2005.07.007 · PMID: 16182563

17. **2dx_automator: Implementation of a semiautomatic high-throughput high-resolution cryo-electron crystallography pipeline**
Sebastian Scherer, Julia Kowal, Mohamed Chami, Venkata Dandey, Marcel Arheit, Philippe Ringler, Henning Stahlberg
Journal of Structural Biology (2014-05) https://doi.org/f522h3
DOI: 10.1016/j.jsb.2014.03.016 · PMID: 24680783

18. **Electron counting and beam-induced motion correction enable near-atomic-resolution single-particle cryo-EM**
Xueming Li, Paul Mooney, Shawn Zheng, Christopher R Booth, Michael B Braunfeld, Sander Gubbens, David A Agard, Yifan Cheng
Nature Methods (2013-06) https://doi.org/f4zpjf
DOI: 10.1038/nmeth.2472 · PMID: 23644547 · PMCID: PMC3684049

19. **Preparation of Primary Neurons for Visualizing Neurites in a Frozen-hydrated State Using Cryo-Electron Tomography**
Sarah H Shahmoradian, Mauricio R Galiano, Chengbiao Wu, Shurui Chen, Matthew N Rasband, William C Mobley, Wah Chiu
Journal of Visualized Experiments (2014-02-12) https://doi.org/gmh9w3

DOI: [10.3791/50783](#) · PMID: [24561719](#) · PMCID: [PMC4089403](#)

20. **Adam: A Method for Stochastic Optimization**
     Diederik P Kingma, Jimmy Ba
     arXiv (2014) https://doi.org/hnkr
     DOI: [10.48550/arxiv.1412.6980](#)